J. Plasma Fusion Res. SERIES, Vol. 6 (2004) 51–59

Recent Results from LHD Experiment with Emphasis on Relation to Theory from Experimentalist's View

YAMADA Hiroshi, IDA Katsumi, WATANABE Kiyomasa, SAKAKIBARA Satoru, INAGAKI Shigeru, MURAKAMI Sadayoshi[1], NARUSHIMA Yoshiro, OHYABU Nobuyoshi, YOKOYAMA Masayuki, YOSHINUMA Mikiro, COOPER W.A.[2], KOBUCHI Takashi, OSAKABE Masaki, TOI Kazuo, SUZUKI Yasuhiro[3], AKIYAMA Takeshi, ASAKURA Nobuyuki[4], ASHIKAWA Naoko, EMOTO Masahiko, FUJITA Takaaki[4], FUJIWARA Masami, FUNABA Hisamitsu, GONCHAROV Pavel, GOTO Motoshi, HAMADA Yasuji, HIGASHIJIMA Satoru[4], HINO Tomoaki[5], HOSHINO Mitsuyasu[6], ICHIMURA Makoto[7], IDEI Hiroshi[8], IDO Takeshi, IKEDA Katsunori, ISAYAMA Akihiko[4], ISOBE Mitsutaka, ITOH Takafumi[6], ITOH Kimitaka, KADO Shinichiro[9], KALININA Diana[10], KANEBA Takahiro[10], KANEKO Osamu, KAWAHATA Kazuo, KAWAZOME Hayato[3], KONDO Katsumi[3], LYON J.F.[11], MASE Atsushi[8], MASUZAKI Suguru, MATSUOKA Keisuke, MIURA Yukitoshi[4], MIYAZAWA Junichi, MORISAKI Tomohiro, MORITA Shigeru, MUTO Sadatsugu, MUTOH Takashi, NAGAOKA Kenichi, NAGASAKI Kazunobu[3], NAGAYAMA Yoshio, NAKAMURA Yukio, NAKANISHI Hideya, NARIHARA Kazumichi, NISHIMURA Kiyohiko, NISHIURA Masaki, NISHIZAWA Akimitsu, NODA Nobuaki, NOTAKE Takashi[6], NOZATO Hideaki[9], OHDACHI Satoshi, OHKUBO Kunizo, OYAMA Naoyuki[4], OKA Yoshihide, OKADA Hiroyuki[3], OZAKI Tetsuo, PETERSON Byron J., SAGARA Akio, SAIDA Tomoya[12], SAITO Kenji, SAKAMOTO Mizuki[8], SAKAMOTO Ryuichi, SASAO Mamiko[12], SATO Kuninori, SEKI Tetsuo, SHIMOZUMA Takashi, SHOJI Mamoru, SUDO Shigeru, TAKAGI Shoji, TAKAHASHI Yoshiyuki, TAKASE Yuichi[9], TAKEIRI Yasuhiko, TAKENAGA Hidenobu[4], TAKEUCHI Norio[6], TAMURA Naoki, TANAKA Kenji, TANAKA Masayoshi, TOKUZAWA Tokihiko, TORII Yuki[6], TSUMORI Katsuyoshi, WATANABE Fumitake[6], WATANABE Tsuguhiro, WATARI Tetsuo, YAMADA Ichihiro, YAMAGUCHI Taiki[10], YAMAMOTO Satoshi[3], YAMAZAKI Kozo, YOSHIDA Naoaki[8], YOSHIMURA Shinji, YOSHIMURA Yasuo, KOMORI Akio and MOTOJIMA Osamu

National Institute for Fusion Science, Toki, 509-5292, Japan
[1]Kyoto University, Kyoto, 606-8501, Japan
[2]CRPP, Ecole Polytechnique Federale de Lausanne, Switzerland
[3]Kyoto University, Uji, 611-0011, Japan
[4]Japan Atomic Energy Research Institute, Naka Fusion Research Establishment, Ibaraki, 311-0193, Japan
[5]Hokkaido University, Sapporo, 060-8628, Japan
[6]Nagoya University, Nagoya, 464-8603, Japan
[7]Tsukuba University, Tsukuba, 305-8577, Japan
[8]Kyushu University, Kasuga, 816-8580, Japan
[9]The University of Tokyo, Tokyo, 113-8658, Japan
[10]Graduate University for Advanced Studies, Kanagawa, 240-0193, Japan
[11]Oak Ridge National Laboratory, Oak Ridge, TN, USA
[12]Tohoku University, Sendai, 980-8579, Japan

(Received: 6 January 2004 / Accepted: 11 March 2004)

Abstract

The Large Helical Device (LHD) has been extending an operational regime of net-current free plasmas towards the fusion relevant condition with taking advantage of a net current-free heliotron concept and employing a superconducting coil system. Heating capability has exceeded 10 MW and the central ion and electron temperatures have reached 7 and 10 keV, respectively. The maximum value of β and pulse length have been extended to 3.2% and 150 s, respectively. Many encouraging physical findings have been obtained. Topics from recent experiments, which should be emphasized from the aspect of theoretical approaches, are reviewed. Those are (1) Prominent features in the inward shifted configuration, i.e., mitigation of an ideal interchange mode in the configuration with magnetic hill, and confinement improvement due to suppression of both anomalous and neoclassical transport, (2) Demonstration of

Corresponding author's e-mail: hyamada@lhd.nifs.ac.jp

bifurcation of radial electric field and associated formation of an internal transport barrier, and (3) Dynamics of magnetic islands and clarification of the role of separatrix.

Keywords:
Large Helical Device, energy confinement, MHD stability, radial electric field, magnetic island, internal transport barrier, magnetic configuration

1. Introduction

Experiments in the Large Helical Device (LHD) have been progressing steadily since the first plasma in 1998 [1]. LHD has a helical heliotron magnetic configuration [2] and employs a fully superconducting magnet system, which provides capability of steady state operation. During 6 experimental campaigns in these 5 years, many encouraging physical observations have emerged in conjunction with engineering demonstration of superconducting and heating technologies [3-6]. Intensive theoretical works have been devoted to the LHD project. Some theoretical predictions have been successfully demonstrated in the experiment and some unexpected but favorable experimental findings have been requiring further progress in theory. Major highlights from recent experiments which attract theoretical interests are reviewed in this article.

The nominal major and minor radii of LHD are 3.9 m and 0.6 m, respectively, which leads to the plasma volume of 30 m^3. The superconducting coil system including the cryogenic and the power supply systems has provided steady-state magnetic field around 3 T routinely. A pair of helical coils consists of 3 layers with independent power supply. The aspect ratio of the plasma and rotational transform can be controlled by coordinating coil currents in each layer. Three sets of poloidal coils can change the position and the shape of the plasma column. In particular, the position of the magnetic axis has distinguished effect on both transport and MHD (magneto-hydro-dynamics) stability. In addition to these main superconducting coils, LHD has ten pairs of perturbation coils which can generate low-order magnetic islands in the plasma. This experimental set-up provides large flexibility of magnetic configuration. The available heating source has been extended to 10.3 MW of NBI (Neutral Beam Injection), 2.1 MW of ECH (Electron Cyclotron Heating) and 2.7 MW of ICH (Ion Cyclotron Heating). The NBI system is equipped with three tangential negative-ion-based neutral beam injectors and the nominal injection energy is as high as 180 keV [7]. The microwave sources used for ECH are two 84 GHz gyrotrons, two 82.7 GHz gyrotrons and three 168 GHz gyrotrons [8]. Six ICRF (Ion Cyclotron Resonant Frequency) antennas of a single center strap have been installed at the three toroidal sections [9].

In the following sections, first the outline of recent progresses is described briefly. Then, three major topics are presented, i.e., (1) prominent feature in the configuration with the inward shifted magnetic axis, (2) observation of bifurcation of radial electric field and associated formation of internal transport barrier, and (3) effect and dynamics of magnetic islands.

More detailed reports related to LHD experiment can be found in several articles in the current issue.

2. Outline of progress

Along with growth of heating capability, plasma parameters have been progressing steadily. The plasma stored energy has reached 1.25 MJ, which is catching up leading large tokamaks. Also central electron and ion temperatures have reached 10 keV and 7 keV, respectively and the maximum pulse length has been beyond 2 min. The maximum values of β and density to date are 3.2% and 1.6×10^{20} m^{-3}, respectively [6]. In particular, high β discharges have been demonstrated in the region where a linear MHD stability theory predicts growth of an interchange mode. Density limit is determined by the power balance and no hard limit like the Greenwald limit in tokamaks has not been recognized [10]. The LHD enables exploration of physics of net-current free plasmas towards fusion relevant regime represented in above mentioned typical plasma parameters. In addition, non-dimensional parameters are of importance as well to get comprehensive physical understanding. Figure 1 shows the achieved regime in the primarily important non-dimensional

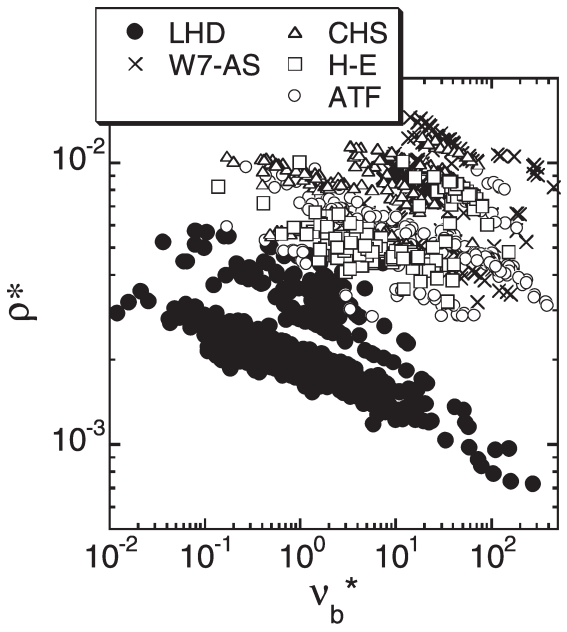

Fig. 1 Operational regime of net-current free plasmas in helical experiments (LHD, W7-AS, ATF, CHS and Heliotron E) on the plane of normalized gyro radius ρ* and collisionality ν_b*. Here collisionality is normalized by the bounce frequency in a banana orbit.

parameters, i.e., normalized gyro radius ρ^* and collisionality ν_b^*. Data from medium sized helical experiments are also plotted. It can be pointed out that the LHD has largely extended the envelope of the operational regime of net-current-free plasmas. Two major approaches to the reactor regime poses two major subjects. In the direction to low ρ^*, the understanding anomalous transport is a key. Also in the direction to the deep collisionless regime, controlling neoclassical transport is, in particular, important in helical systems.

A database for energy confinement time τ_E in helical systems has advanced with compilation of data from LHD. Figure 2 shows the comparison of experimental data with the prediction from the ISS95 scaling [11],

$$\tau_E^{ISS95} = 0.079 a^{2.21} R^{0.65} P^{-0.59} \bar{n}_e^{0.51} B^{0.83} \iota_{2/3}^{0.4} \propto \tau_B \rho_*^{-0.71} \beta^{-0.16} \nu_*^{-0.04} .$$

Here, a, R, P, $\bar{n}_e$, B and $\iota_{2/3}$ are minor and major radii in the unit of m, heating power in the unit of MW, line averaged electron density in the unit of 10^{19} m^{-3}, and magnetic field in the unit of T, and rotational transform at two thirds radius. Non-dimensional expression of the energy confinement time normalized by Bohm time τ_B indicates that ISS95 is characterized by gyro-Bohm nature and no definitive dependence on β and collisionality. Data from tokamak L-mode and H-mode are also plotted in Fig. 2 and ISS95 gives tolerable fits to both data set. Performance of LHD plasmas has shown improvement upon ISS95 up to a factor of two [12]. This improvement is proved to be due to (1) no enhancement of heat diffusivity in the edge and consequent high edge pressure [13] (2) reduction of heat diffusivity in the core [14]. The former factor seems to be robust characteristics in LHD since the edge pressure at $\rho = 0.9$ can be described by a unique scaling independent of the position of the magnetic axis [12]. Here ρ is the normalized minor radius. In addition to the former factor, the latter factor distinguishes the advantage of the geometry with the inward shift of the magnetic axis from the outward shifted configuration. The upper envelope of data from LHD as well as W7-AS is comparable to tokamak H-mode.

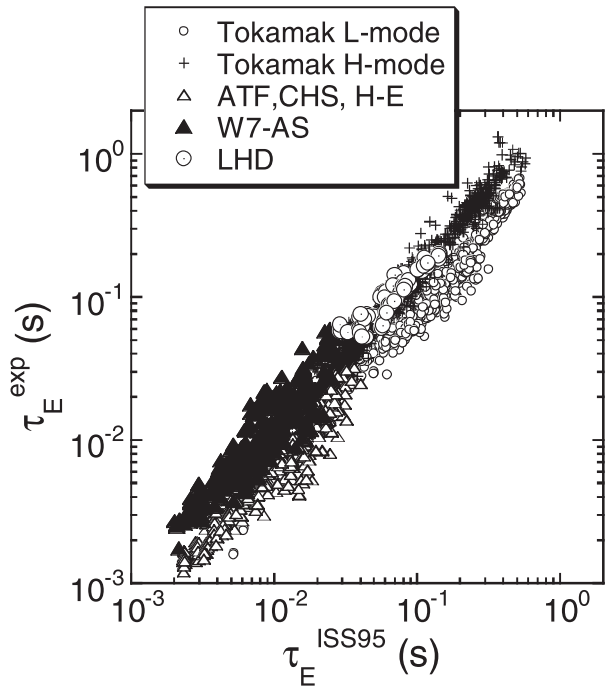

Fig. 2 Comparison of energy confinement in experiments with prediction from the ISS95 scaling.

3. Effect of tailoring magnetic configuration

3.1 Confinement and thermal transport

In the following discussions including MHD nature, the position of the magnetic axis is a key. When the magnetic axis is shifted inward in LHD, the orbit of helically trapped particles fits to the magnetic flux surfaces well. In contrast, deviation between the orbit and flux surface becomes large in the case with outward shift of the magnetic axis. Along with the same direction, a good neoclassical transport can be anticipated in the inward shifted configuration. The scenario to get good confinement in terms of neoclassical transport can be summarized as follows. In the $1/\nu$ regime, a heat flux q is a very strong function of temperature T like $q \approx -\left(\frac{\varepsilon_t}{erB}\right)^2 \varepsilon_h^{1.5} \frac{T^{9/2}}{L_T}$, where ε_t and ε_h are toroidal and helical ripples, L_T is the scale length of the temperature gradient, e is the unit electrical charge, and r is the minor radius. In this regime, super-banana motion of helically trapped particles degrades confinement. This is so called helical ripple transport. By optimizing geometry, an effective helical ripple can be reduced, consequently heat flux can be suppressed [15]. One of the real approaches is the inward shift of the magnetic axis. This scenario is not, however, sufficient to realize good confinement in the deep collisionless regime. Another scenario relies on favorable effect of radial electric field E_r. In the non-axisymmetric system, the radial electric field is determined by the neoclassical ambipolar relation. When the radial electric field is present, the $1/\nu$ regime changes into the collisional detrapping ($\sqrt{\nu}$) regime where $D_{\sqrt{\nu}} \propto \sqrt{\nu}/E_r^{1.5}$ and then the collisionless detrapping (ν) regime where $D_\nu \propto \nu/E_r^2$. The heat flux in the ν regime is expressed by $q \approx -\frac{\varepsilon_t n^2}{E_r^2} \varepsilon_h^{0.5} \frac{T^{3/2}}{L_T}$. When large positive E_r is obtained in the electron root, the heat flux can be reduced significantly. It is pointed out that negative E_r causes degradation of confinement under some circumstances due to helical and/or toroidal resonance [16]. Therefore the electron root is also favorable to avoid this unfavorable resonance.

Figure 3 shows the confinement enhancement factor on ISS95 for the configurations with a different position of the magnetic axis. A distinct confinement improvement by the inward shift (the major radius of the magnetic axis: R_{ax} = 3.6 m) can be seen. Hereafter, this configuration is represented by ISC (Inward Shifted Configuration). Figure 4 shows the confinement enhancement factor as a function of collisionality

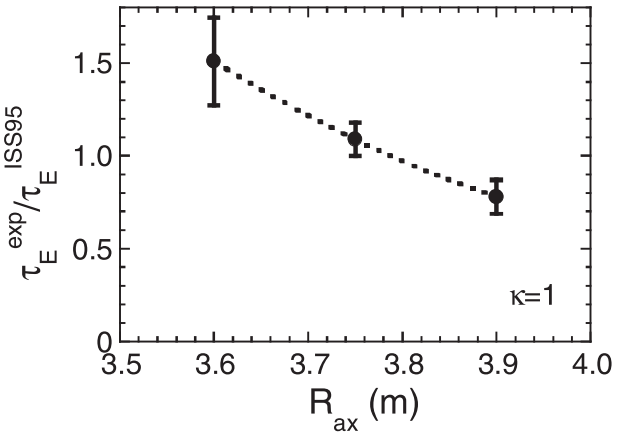

Fig. 3 Confinement enhancement factor on ISS95 for the cases with different magnetic axes (R_{ax} = 3.6 m, 3.75 m, and 3.9 m).

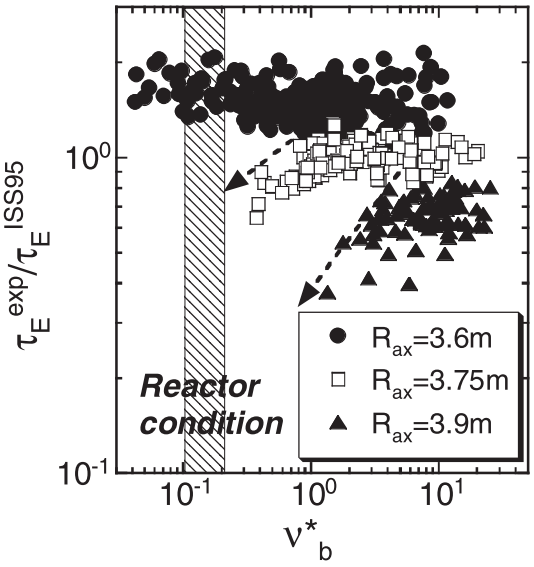

Fig. 4 Confinement enhancement factor is plotted as a function of collisionality (ν_b*) for the cases with different magnetic axes (R_{ax} = 3.6 m, 3.75 m, and 3.9 m).

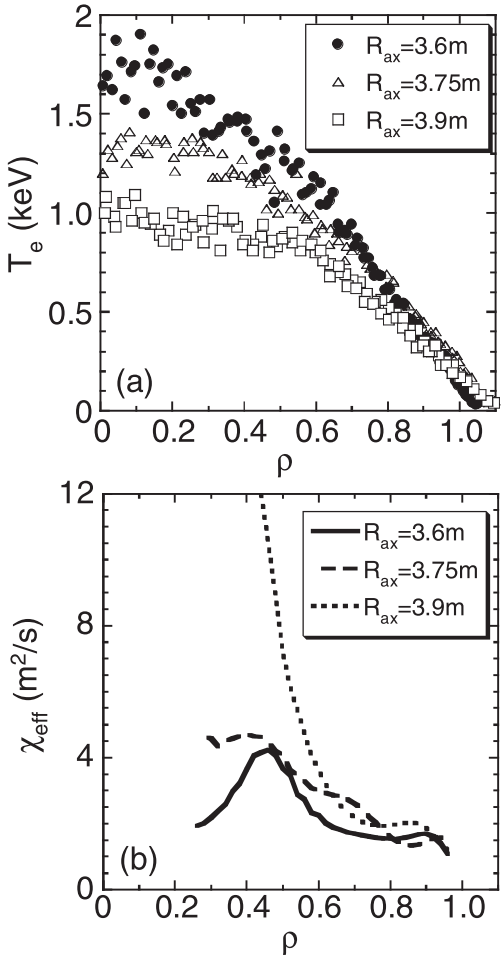

Fig. 5 (a) Electron temperature profiles and (b) Effective thermal diffusivity profiles for 3 cases with different magnetic axes (R_{ax} = 3.6 m, 3.75 m, and 3.9 m). Line averaged density (3.1×10^{19} m^{-3}) and heating power (6.3 MW) are the same for all cases.

for 3 cases with different positions of the magnetic axis. It should be noted that improvement in ISC can be seen in wide collisionality and remains in the collisional regime where the neoclassical transport does not play an essential role. Therefore this geometrical property in ISC causes reduction of anomalous transport [12]. Neoclassical optimization also contributes improvement, which is indeed seen more clearly in the deep collisionless regime in Fig. 4. Confinement degradation dependent on collisionality is observed in the configuration with outward shifted magnetic axis which is not optimized in terms of neoclassical transport in the $1/\nu$ regime. In other words, no distinct dependence of confinement in ISC even in the deep collisionless regime is a demonstration of geometrical optimization for neoclassical transport theory. With regard to anomalous transport, a linear stability of ITG (Ion Temperature Gradient mode)/TEM (Trapped Electron Mode) by the FULL code has been investigated [17], but coherent results have not obtained yet. If a crude argument is allowed, ITG/TEM are more stable in LHD than in tokamak because of shorter connection length between bad and good curvatures [18] and that ITG/TEM are more unstable in the inward shifted configuration because of bad curvature due to magnetic hill.

Figure 5 shows the profiles of electron temperature and effective thermal diffusibity in the discharges with different magnetic axis. Besides the position of magnetic axis, major parameters are fixed on the same condition. Line averaged density is the same at 3.1×10^{19} m^{-3} although there is some structural difference in the profile. The deposited power is also the same at 6.3 MW and the deposition profiles are quite similar to each other. Nonetheless, pronounced difference in electron temperature can be seen (see Fig. 5(a)). The central temperature is doubled when the axis is shifted inward from 3.9 m to 3.6 m. This confinement enhancement is distinguished in the core region within ρ of 0.7 while the peripheral region does not show any significant difference.

Improvement of thermal transport in ISC is clear in the core region although all cases are located at the same level in the peripheral region (see Fig. 5(b)). In the second section, confinement enhancement in LHD is compared with medium sized heliotrons (ATF, CHS and Heliotron E). Compared with the medium sized experiments, the scale merit beyond the size scaling in LHD has been found. It is due to high edge pressure. The thermal diffusivity is not deteriorated even close to the boundary. This leads to confinement enhancement of factor of 1.8 in LHD on medium sized heliotrons. In addition, further improvement in the core region by ISC results in the confinement enhancement factor of up to 2.6.

3.2 MHD stability

In LHD, it has been mentioned that ISC, i.e., R_{ax} = 3.6 m has better confinement properties when the confinement performance is evaluated based on the ISS95 global energy confinement scaling [11]. From a viewpoint of high-energy particle confinement properties, the configuration with the magnetic axis shifted inward is considered to be a better configuration. Also, from a viewpoint of the MHD equilibrium limit, ISC provides room for the Sharanov shift and consequently yields the higher equilibrium β limit. On the contrary, in heliotron devices, ISC has been considered to be unfavorable from a viewpoint of MHD stability because of enhanced magnetic hill. However, the MHD instability of ISC is found to be much mitigated from the prediction of a linear stability theory in the experiment. Volume average β's of 3.2% with pellet and of 3% by gas puffing have been achieved without any disruptive phenomena. Magnetic axis shift with $\Delta R/a_p \sim 50\%$ are observed in $\langle\beta\rangle \sim 2.5\%$. Abrupt declination of global energy confinement time against β has not been observed below $\langle\beta\rangle \sim 3.2\%$.

LHD has a strong magnetic shear, and there are many low order rational surfaces from ι = 2/5 to 3/2. Nonetheless, ι = 1/2 and ι = 1/1 rational surfaces are considered as typical rational surfaces at the core and the edge, respectively, where ι = 1/2 and ι = 1/1 rational surfaces are located at $\rho \sim 0.5$ and $\rho \sim 0.9$, respectively. Figure 6 (a) shows the experimentally observed pressure gradients at ρ = 0.5 in R_{ax} = 3.6 m configuration with $\langle\beta\rangle$-dβ/dρ diagram. Solid and dashed lines denote the stability boundaries for low-n ideal mode and Mercier mode, respectively [19]. The low-n ideal MHD unstable region is calculated by a 3-D MHD stability analyzing code (TERPSICHORE [20]). Here, the growth rate of a low-n ideal MHD mode, $\gamma_{low\text{-}n} = 10^{-2}\ \omega_A$ is defined as the stability boundary, which corresponds to Mercier parameter [21], $D_I \sim 0.25$. Here ω_A is the Alfvén frequency. It should be noted that the stability boundary based on the low-n mode analysis is considered as that for global modes, and that the Mercier condition, $D_I = 0$, corresponds to the stability boundary for localized modes [22]. When plasmas approach the high β regime, the achieved pressure gradients look to avoid the low-n linear ideal MHD mode unstable region in the core. Although most of the experimentally observed pressure gradients do not enter the low-n unstable

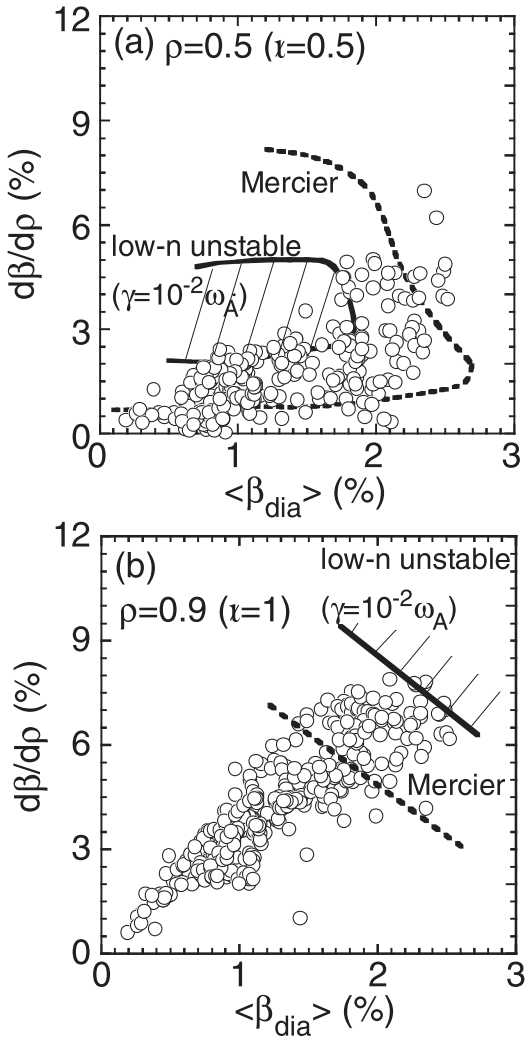

Fig. 6 Evolution of pressure gradient at core ((a) ρ = 0.5) and at periphery ((b) ρ = 0.9) with the increase of β. The dotted line is the boundary of Mercier criterion and hatched regionis low-n ideal MHD unstable region predicted from the calculation by TERPSCICHORE [18].

region, they do not seem to be limited by the Mercier condition. In particular, low-n unstable region disappears at $\langle\beta\rangle$ = 1.8% due to spontaneous formation of magnetic well, the pressure gradient evolves more than twice larger than those below $\langle\beta\rangle$ = 1.8%. The amplitude of the resonant magnetic fluctuation (m/n = 2/1) increases as dβ/dρ increases. Then the increment of the amplitude becomes smaller in $\langle\beta\rangle$ = 1 ~ 1.8% once, where the β-gradients are saturated against β, than in other β region. The resonant fluctuation in the core has not been observed in the β region of $\langle\beta\rangle < 0.3\%$ and $\langle\beta\rangle > 2.3\%$, where corresponds to Mercier stable region [23]. Figure 6(b) shows the experimentally observed pressure gradients at ρ = 0.9 in R_{ax} = 3.6 m configuration with $\langle\beta\rangle$-dβ/dρ diagram [19]. The upper limit of the achieved pressure gradients at ρ = 0.9 in the profile data analyzed here is located at the beginning of the unstable region. At the edge region, it is still unclear whether the low-n ideal mode limits the pressure gradients because the experimentally achieved β

is not still enough high to make clear it. On the contrary, the β-gradients does not seem to care the Mercier condition in the edge as well as in the core.

There exists an experimental observation suggesting a sign of effect of low-n modes on a plasma discharge. Figure 7 is a waveform of a typical high-β discharge [24]. In this case the m/n = 2/1 mode which has the resonance in the core is pretty quiet. However, the burst of modes localized in the periphery and the edge start over β of 2.3%, and the stored energy and confinement seem to hesitate about further evolution. Also it should be noted that m/n = 2/3 mode has no resonant surface at least in the vacuum calculation. Possibility of healing of the ergodic region in the edge or excitation of external mode should be considered [25].

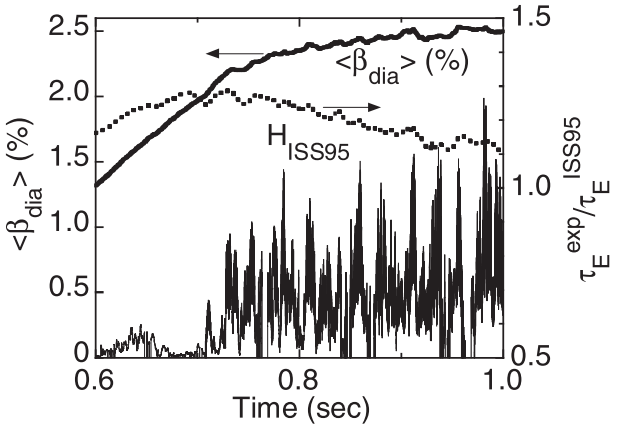

Fig. 7 Waveforms of a high β discharge. A solid curve is β, a dotted curve is a confinement enhancement factor on ISS95, and a thin solid curve is an amplitude of magnetic fluctuation of m = 2/n = 3 mode [23].

4. Observation of bifurcation of radial electric field and associated formation of internal transport barrier

Importance of radial electric field, in particular, in non-axisymmetric configuration, has been recognized widely. Understanding of bifurcation mechanism of E_r is progressing in the LHD experiment. A highlighted event attracting both experimental and theoretical interest is the transition from the ion root to the electron root in collisionless plasmas. This event is predicted by the neoclassical ambipolar condition, i.e., balance between the electron flux Γ_e and the ion flux Γ_i [26]. A theoretical calculation for the radial electric field in the edge region is shown in Fig. 8 (a) [27]. In this calculation, the temperature is fixed and the density is scanned. Therefore the horizontal axis can be rephrased into collisionality. Here three configurations with different magnetic axis position are plotted. In the high density regime, only one ion root exists. As the density decreases, namely, collisionality decreases, multi-roots come up and transition to the electron root becomes possible. The threshold density, which is equivalent to collisionality, depends on configuration. In ISC, transition density is quite low since asymmetric flux is suppressed. Figure 8 (b) is the corresponding experimental observation on the same diagram [27]. In ISC, the plasma remains in the ion root. In contrast, the electron root is formed in the case of outward shifted configuration. In the case between them, the plasma wanders in the halfway. It is also pointed out that improvement of heat transport is clarified experimentally in the case with large neoclassical transport [28].

High electron temperature has been achieved through formation of an internal transport barrier (ITB) [29] associated with the transition from the ion root to the electron root [26]. When the central ECH is applied to NBI target plasmas, abrupt formation of ITB by tiny increase of ECH power has been observed. Figure 9 (a) shows the electron temperature

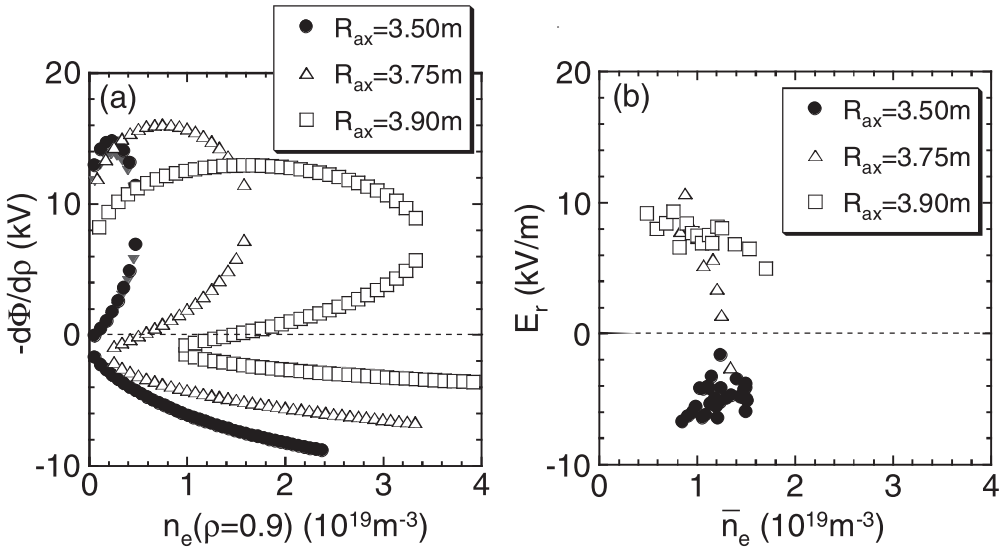

Fig. 8 Radial electric field is plotted as a function of density for the cases with different magnetic axes (R_{ax} = 3.5 m, 3.75 m, and 3.9 m). (a) Calculation based on neoclassical transport. (b) Experimental observation [26].

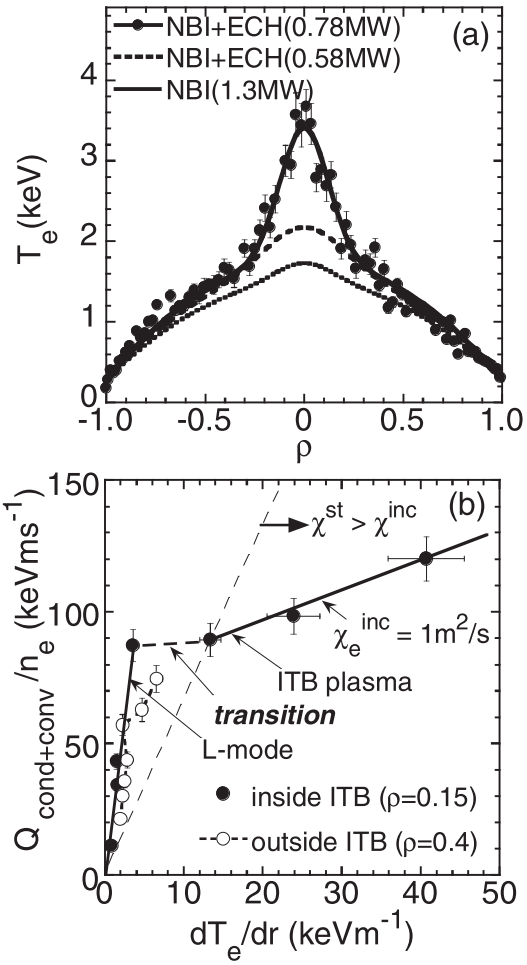

Fig. 9 Formation of internal transport barrier. (a) Electron temperature profiles for different heating conditions. (b) Normalized heat conductions of inside ITB (ρ = 0.15) and outside ITB (ρ = 0.4) is plotted as function of the temperature gradient [29].

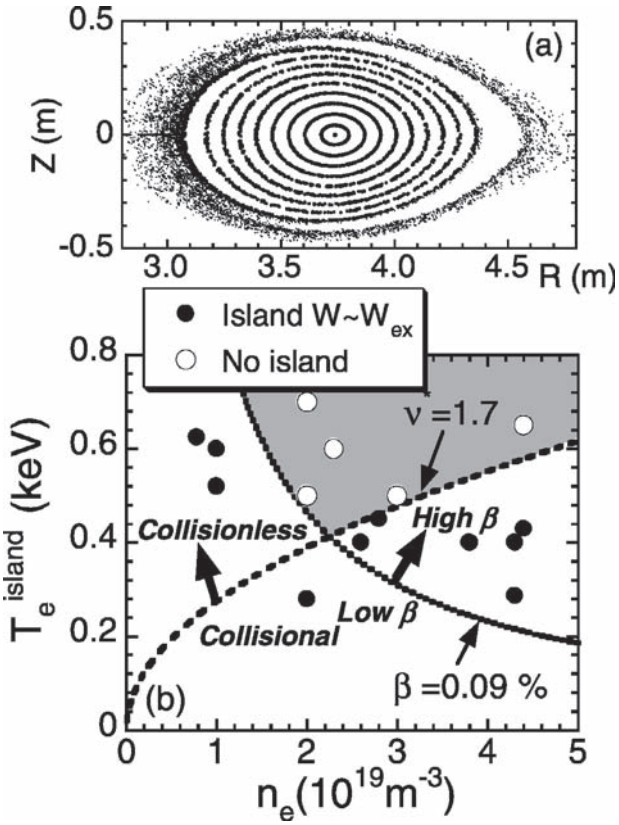

Fig. 10 Plasma response to externally generated magnetic island of m = 1/n = 1. (a) Field line calculation of vacuum magnetic field. (b) Parameter space (T_e^{island}, n_e) for island suppression. Open circles are the cases with no detectable island. Solid circles are the cases with a visible island in electron temperature profile [30].

profiles. NBI target plasma is shown in a dotted curve [30]. A broken curve is the case of ECH power of 0.58 MW. Increase of only 200 kW of ECH power pushes the central electron temperature by more than 50% and a large temperature gradients appears near the plasma center at $\rho <$ 0.3. The radial profiles of E_r are derived from poloidal flow velocity v_θ measured with charge exchange spectroscopy (CXS) using fully ionized Neon (0.5–1%) impurity [28]. The transition of E_r from small positive value to the large positive value is observed at $\rho < 0.4$ when the ECH power exceeds the threshold. In the case with the collisionality ν_b^* (ρ = 0.27) > 0.3, there has not been observed transition of E_r and increase of temperature gradient.

The formation of the electron internal transport barrier is due to the bifurcation phenomena of the electron heat transport, which is clearly demonstrated in the relation between the electron heat flux normalized by density and temperature gradient as seen in Fig. 9 (b) [30]. Here, the relation between the temperature gradient and heat flux, especially incremental χ_e^{inc} [= $(1/n)\mathrm{d}q/\mathrm{d}(\nabla T)$] in the plasma with ITB at significant low collisionality regime $\nu_b^* < 0.2$ are discussed. Reduction in heat diffusivity by a factor of 5–10 inside the ITB has been confirmed by a power scan and a heat/cold pulse propagation scheme. The transport analysis shows that the χ_e^{inc} in the plasma with ITB is 1 m^2/s, which is much lower than that without ITB by more than an order of magnitude. Because of $\chi_e^{inc} < \chi_e$, the χ_e decreases as the heat flux is increased inside the ITB (confinement enhancement). It should be noted that the heat transport in ITB is still anomalous and it is reasonable that anomalous transport is suppressed by E_r or its shear.

5. Magnetic island

The final topic is related to effect of magnetic topology. As mentioned in introduction, LHD has a capability to generate a resonant island externally as seen in Fig. 10 (a). The response of plasma to this island is attracting interests, in particular, in comparison with a neoclassical tearing mode in tokamaks. Usually, local flattening in temperature profile corresponding to this island is observed. In specific condition, however, this island becomes invisible. In Fig. 10 (b) [31], the existence of magnetic island is summarized in the parameter space on the temperature and density where the island should be located. Solid circles indicate that the island is visible in the temperature measurement. In contrast, open

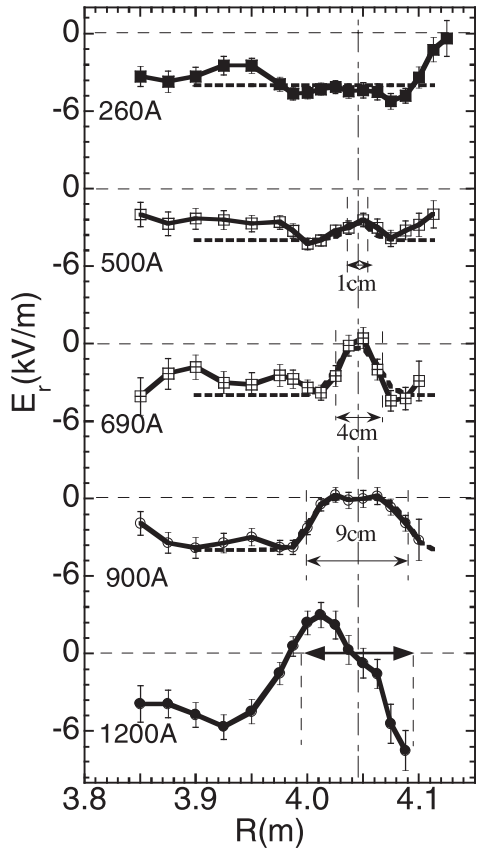

Fig. 11 Effect of externally generated magnetic island on radial electric field profile. Island width is gradually enlarged from the top to the bottom by increasing the current of the perturbation coil [31].

circles are invisible cases where the island is suppressed. If a crude experimentalist's insight is allowed, the parameter space is divided by two curves, which leads to the idea that the island is healed in the high-β and collisionless regime.

Figure 11 shows another aspect of a function of magnetic islands. Electric potential profiles are derived from the poloidal rotation of the plasma [32]. The resonance of the external perturbation (m/n = 1/1) is located at 4.05 m. The magnetic island width is enlarged by increasing currents in the perturbation coil from the top to the bottom. When the island is small, flattening of potential in the island is observed. When the island width is increased further, a clear poloidal flow in the island is generated and specific potential structure appears (the bottom case). This dynamics indicates that topological interface (separtrix of the magnetic island) has a potential to generate large E_r shear, eventually linking to possibility of confinement improvement.

Since the temperature profile in the magnetic island is usually flat, heat transport in the island cannot be evaluated in a steady state manner of power balance analysis. Therefore transient transport analysis is prerequisite. LHD provides an excellent experimental platform of this study since a large static island which does not rotate can be generated. By controlling the phase of the island, cold pulse propagation inside and outside the island is investigated. Figure 12 (a) shows the cold pulse propagation in the island [33]. In this case, the tracer encapsulated solid pellet [34] is injected through the X point of the island to induce a cold pulse. Temperature evolution after that is measured along the chord crossing the O point by ECE (Electron Cyclotron Emission) diagnostics. In contrast, Fig. 12 (b) is the case with the pellet deposited in the island and ECE measurement passing through the X point [33]. A simulation result based on simple diffusive

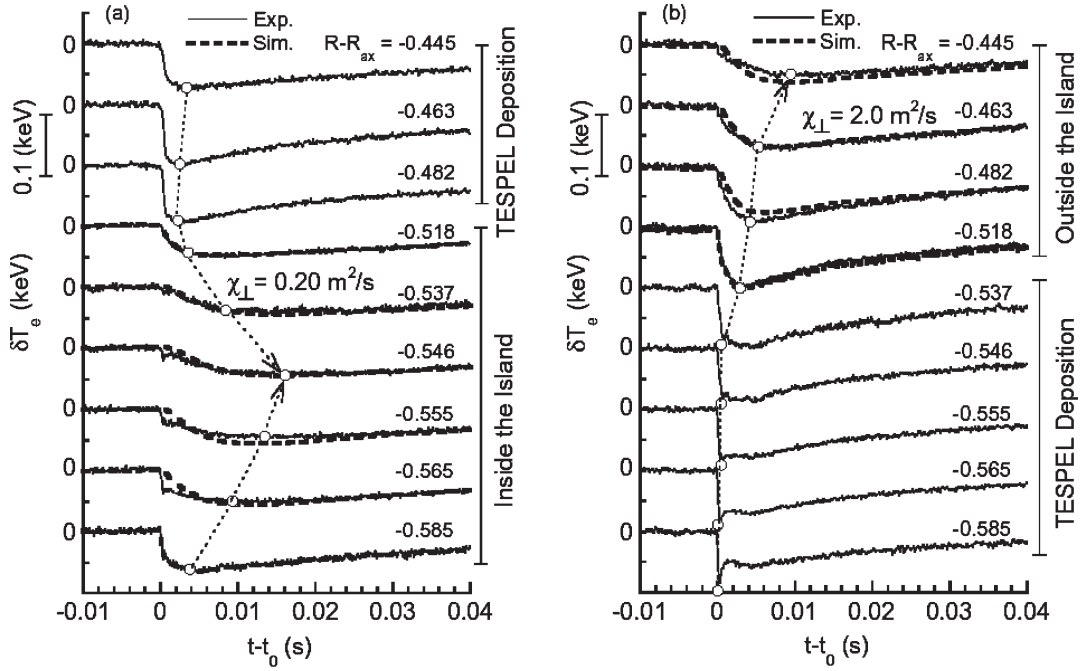

Fig. 12 Cold pulse propagation (a) inside the magnetic island and (b) outside the magnetic island [32].

model is also illustrated in Fig. 12. From this analysis, the heat transport in the magnetic island is found to be significantly reduced by a factor of more than 10.

6. Summary

The LHD has been extending an operational regime towards fusion relevant condition with taking advantage of a net current-free heliotron concept and employing a superconducting coil system. Heating system has been upgraded and available power has exceeded 10 MW, which has enhanced plasma parameters. Many encouraging physical findings have been obtained, ex., simultaneous achievements of mitigation of MHD instability criteria and good confinement, and formation of internal transport barrier. Some highlight data should be emphasized in terms of theoretical approaches. Mitigation of an ideal interchange mode in the configuration with magnetic hill remains a challenging issue. Nonlinear process of growth of instability or stabilization effect [35] which has not been incorporated in the presently available model should be explored. Confinement improvement due to suppression of both neoclassical and anomalous transport has been realized simultaneously by ISC. The former (neoclassical) achievement is a successful demonstration of the theory but a coherent theoretical understanding for the latter (anomalous) achievement has not been available yet. Regarding bifurcation of the radial electric field, a qualitative agreement with neoclassical theory has been obtained and quantitative argument is being available. ITB formation has a close relation to this mechanism. Confinement of high energy particles can be also characterized by an available theory (3-D simulation [36]) well and a quantitative argument with the experiment is in scope although it is not described in this paper. LHD provides an experimental platform to verify innovative attempts with regard to the effect of magnetic topology, ex. dynamics of magnetic island, role of sepratrix, etc. with taking advantage of large flexibility of magnetic configuration.

Acknowledgements

A number of national and international collaborations in a wide spectrum for the LHD project are acknowledged. The authors wish to thank all technical stuff of the LHD group for their helpful support during this work.

References

[1] A. Iiyoshi *et al.*, Nucl. Fusion **39**, 1659 (1999).
[2] K. Uo, J. Phys. Soc. Jpn. **16**, 1380 (1961).
[3] O. Motojima *et al.*, Nucl. Fusion **40**, 599 (2000).
[4] O. Motojima *et al.*, Phys. Plasmas **6**, 1843 (1999).
[5] M. Fujiwra *et al.*, Nucl. Fusion **41**, 1355 (2001).
[6] O. Motojima *et al.*, Nucl. Fusion **43**, 1674 (2003).
[7] O. Kaneko *et al.*, Nucl. Fusion **42**, 692 (2003).
[8] T. Shimozuma *et al.*, Fusion Eng. Des. **53**, 525 (2001).
[9] T. Mutoh *et al.*, Nucl. Fusion **43**, 738 (2003).
[10] Y. Xu *et al.*, Nucl. Fusion **42**, 601 (2002).
[11] U. Stroth *et al.*, Nucl. Fusion **36**, 1063 (1996).
[12] H. Yamada *et al.*, Plasma Phys. Control. Fusion **43**, A55 (2001).
[13] H. Yamada *et al.*, Phys. Rev. Lett. **84**, 1216 (2000).
[14] H. Yamada *et al.*, Nucl. Fusion **41**, 901 (2001).
[15] S. Murakami *et al.*, Nucl. Fusion **42**, L19 (2002).
[16] H. Sanuki, J. Todoroki and T. Kamimura, Phys. Fluids B **2**, 2155 (1990).
[17] G. Rewoldt *et al.*, Nucl. Fusion **42**, 1047 (2002).
[18] T. Kuroda *et al.*, J. Phys. Soc. Jpn. **69**, 2485 (2000).
[19] K.Y. Watanabe *et al.*, *this conference*.
[20] W.A. Cooper *et al.*, Plasma Phys. Control. Fusion **34**, 1011 (1992).
[21] A.H. Grasser *et al.*, Phys. Fluids **18**, 143 (1975).
[22] M. Wakatani *et al.*, Fusion Eng. Des. **15**, 395 (1992).
[23] S. Sakakibara *et al.*, Nucl. Fusion **41**, 1177 (2001).
[24] S. Sakakibara *et al.*, *submitted to* J. Plasma Fusion Res.
[25] N. Nakajima *et al.*, *this conference*.
[26] M. Yokoyama *et al.*, J. Plasma Fusion Res. **79**, 816 (2003).
[27] M. Yokoyama *et al.*, *this conference*.
[28] K. Ida *et al.*, Phys. Rev. Lett. **86**, 5297 (2001).
[29] Y. Takeiri *et al.*, Phys. Plasmas **10**, 1788 (2003).
[30] K. Ida *et al.*, Phys. Rev. Lett. **91**, 085003 (2003).
[31] N. Ohyabu *et al.*, Phys. Rev. Lett. **88**, 055005 (2002).
[32] K. Ida *et al.*, Phys. Rev. Lett. **88**, 15002 (2002).
[33] S. Inagaki *et al.*, Phys. Rev. Lett. *in printing*.
[34] S. Sudo *et al.*, Plasma Phys. Control. Fusion **44**, 129 (2002).
[35] K. Ichiguchi *et al.*, Nucl. Fusion **43**, 1101 (2003).
[36] S. Murakami *et al.*, J. Plasma Fusion Res. SERIES **5**, 620 (2003).